U.S Department of Energy Collegiate Wind Competition:

Technical Design Report 2022

Written by:

Anthony Butler

William Laurent

Aaron Breitinger

Jacob Piña

Jacob Nelson

Kenny Shin

Jackelyn Garcia

Quinton Cacal

Sidharth Kumar

Miles Krauter

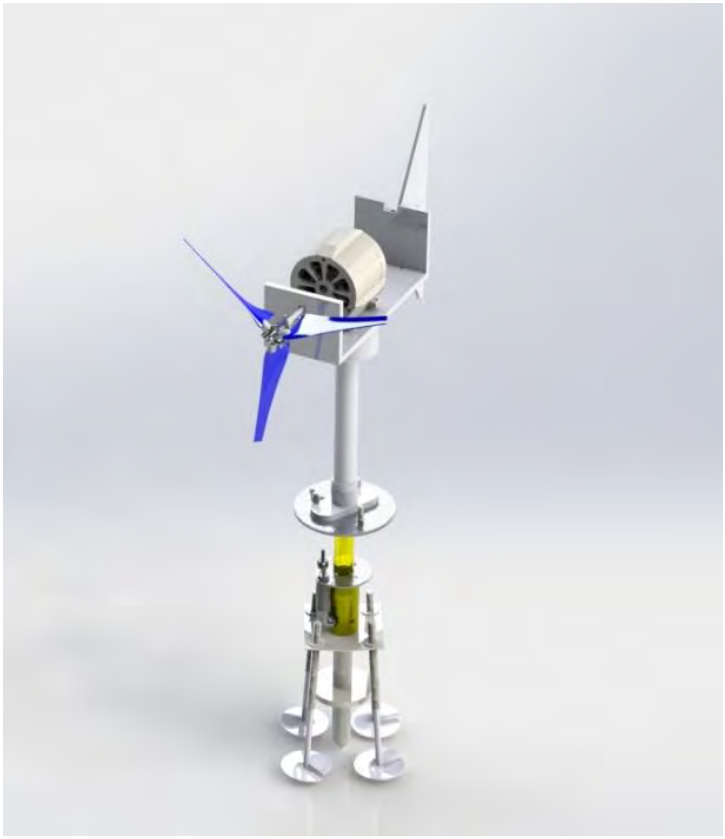

Project Advisors: Dr. Tom Nordenholz, Dr. Tomas Oppenheim, Professor Steffan Long, Erin Cole

CSU – Maritime Academy

April 24, 2022

1 Executive Summary

This year's team's focal point centered upon the offshore aspect of the competition by designing a rigid, lightweight, and unique foundational support. The foundation design this year is a combined four-anchor quadpod and monopile foundational support. From the foundation and up, this year's team took inspiration from previous Cal Maritime teams by incorporating a fully functional variable pitch turbine, with minor design improvements. The turbine this year features a 3-blade variable pitch design, a custom generator, a resistive load, a passive yaw system, and a combined four-anchor quadpod and monopile foundational support.

The foundation design is a quadpod structure that consists of four helical anchors that burrow into the sand. A monopile and baseplate are also incorporated to the structure to add additional stability. The monopile sits below the sand while the plate rests on the sand surface. The plate not only provides more stability but also levels the entire structure. An impact wrench is utilized to screw the anchors into the sand for quick installation.

The airfoils selected for this year's blade were the GOE 497 and GOE 190 airfoils. Using two airfoils from the same family allows us to blend the shapes easily. Utilizing the best performing family of airfoils according to airfoiltools.com, promising tests on campus, and inspiration from previous years teams there are multiple reasons to be confident in the power output with higher wind speeds in competition.

The variable pitch design is the turbine's primary method of controlling power output and rotor speed. The mechanical system results in overall electronic complexity and power consumption with full passive-system control. The operation of pitching the blades will be controlled by a linear actuator mounted in the nacelle. A focus that this year's team had on the variable pitch design was to increase the rigidity and strength of each component, primarily by increasing the depth of connections and overall volume without sacrificing the working efficiency.

The generator for this year's team was inspired by two prior years of successful homemade generator builds out of PLA. In the previous semester, the students involved in the generator design received firsthand experience in building their own generators and experienced the strengths and weaknesses of the two main types: axial flux and radial flux. Axial flux generators direct the flux parallel to the shaft, while radial flux directs it perpendicular to the shaft. The former produces much more power per unit volume but is much more difficult to construct. Ultimately, we believed that radial flux would be the best choice to make use of the Halbach array, which will be explained in greater detail in the generator section.

The electronics system for this year's turbine was inspired from previous year's designs as well. Due to the simplicity of the circuity, and the effectiveness, this year's team proceeded to reincarnate the

electronics system with minor design improvements. Having 2 separate microcontrollers for Load and Turbine side controls, the system controls the variable pitch design according to the output power of the generator, as well as maintaining control power for the system. Changes this year include upsizing the smoothing capacitors on the turbine side to competition limits to add uptime of the microcontroller and pitch actuator during turbine shutdowns, as well as a new 6V supply voltage for the Linear Actuator.

2 Aerodynamics

2.1 Airfoils

All our airfoils were sourced from airfoiltools.com, a website that has 1638 airfoils in its database and that can be easily filtered to our specific situation. For example, the main filter we used when searching for airfoils was the "Max CL/CD @ Re=50,000" filter. We know we can assume a Re of 50,000 because the 2021 team conducted an experiment to see what the Reynolds number is relative to the radial position of the blade. From this search there was a family of airfoils that was more frequently shown, and this was the GOE family of airfoils. It is much easier to transfer airfoils from the same family, and because there were so many, this would be the family of airfoils we would use to create our blades. For our blade design we will be using 3 airfoils, a base airfoil to serve as the strength of the blade, a performance airfoil which will make up most of the blade to obtain the best power output, and a middle airfoil which was a mixture of both, to get a smoother transition between the airfoils.

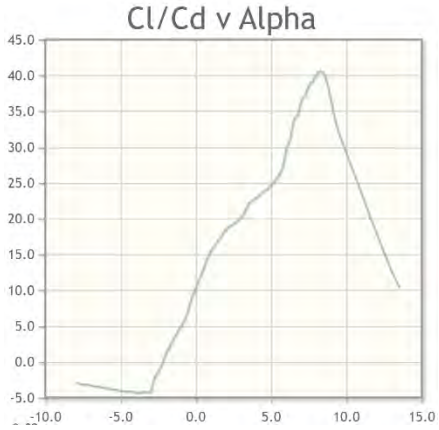

Figure 2-1 Cl/Cd vs. Alpha GOE 190

Our blade design utilized the GOE 497 and GOE 190 airfoil. With these airfoils we were able to keep structural integrity of the base since the GOE 497 had a Max thickness 12.7% at 30% chord. The power airfoil was chosen for its was selected due to its maximum C_L/C_D value of 40.1, and thickness of 8.6% of chord.

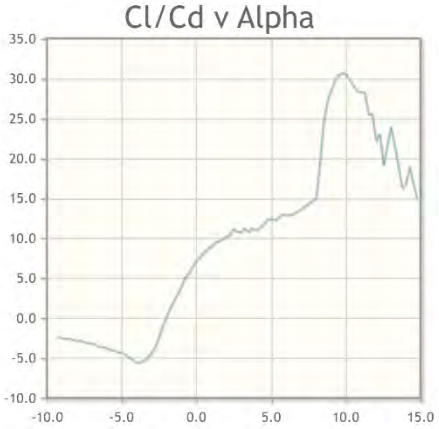

Figure 2-2 Cl/Cd vs. Alpha GOE 497

2.2 Optimization

There are two optimization methods, the Schmitz method and the Betz method. The main difference between these two methods is that the Betz method only accounts for axial downstream losses, while the Schmitz method accounts for axial losses as well as downstream swirl losses due to the rotation of the turbine wake. Because the Schmitz method accounts more accurately for losses, it will be used for all blade designs from start to finish.

The Schmitz optimization method uses a series of equations to determine the ideal chord and twist of the blade along predetermined sections of the blade body to maximize the power captured from the wind. In our case we have divided our blade design into 40 sections of either the base, middle, or power airfoil. By inputting the number of blades, alpha for each section, TSR, C_L, and hub dimensions into our excel sheet we can obtain our chord and twist for each section.

The chord and twists we get from our optimization are imported into Qblade. QBlade is an open-source wind turbine calculation software, distributed under the GPL that utilizes XFOIL which allows users to design unique blade designs and analytically compute performance polars. Being able to simulate blade designs allows us to quickly compare turbine performance, rather than having to physically test each one. Once we have created a blade design that simulates well, we can 3D print the design and physically test the blade in our on-campus wind tunnel.

2.3 Performance

Qblade was also used to find theoretical performance curves. An important analysis conducted was that of the full blade and rotor designs, which utilized the BEM analysis aspect of Qblade. This included a graph of coefficient of power (C_P) vs tip speed ratio (TSR), at different pitch angles for the GOE blade. Each line represents a different pitch angle varying from zero to negative forty-five-degree increments, a negative pitch represents the leading edge towards the wind direction, known as feathering. These graphs were used

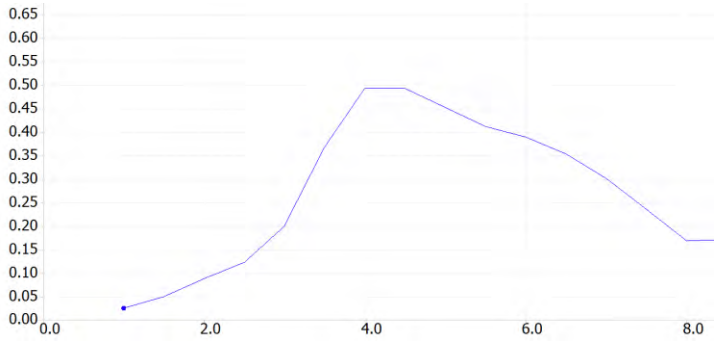

Figure 2-3 C_P vs TSR

2.4 Stress

The blades experience the highest amounts of stress and forces when the turbine is operating at peak rotational speeds. During the 2021 teams testing, the turbine was reaching speeds of about 3000 revolutions per minute in our wind tunnel which only reaches speeds of 16 m/s. To calculate each blade's maximum loading, we analyzed each blade as if the rotor was operating at peak rotational speeds (3000 RPM). QBlade outputs the flap wise aerodynamic force distribution experienced by each blade as well as the blade's geometry into excel. Based on this, the bending moment and axial forces (due to centrifugal loading) are calculated at each of the 40 blade sections at their given radius (r). The axial force (F) across each section could be determined by multiplying the mass of the blade from the section at r to the tip and its centripetal acceleration (A_r)so that ($F = mA_r$). The centripetal acceleration was approximated using the following equation

$$A_r = \frac{(R + r)\omega^2}{2}$$

Equation 2-1

R represents the outer radius of 0.225m, r the radius of each section along the blade body in meters, and ω the speed of the blades in radians/s which needs to be converted from RPM. From here the stress at each blade section could be found by dividing the axial force (F) by the r of each section, which is the stress due to centrifugal loading

To determine the total flap wise deflection and the max stress of the blade under these wind conditions, the shear and bending moment needed to be calculated along each of the 40 sections. The shear could be found by integrating the flap wise aerodynamic loading, F_n, found in Qblade across each r to the outer radius R. The bending moment is found by integrating the shear in the same manner.

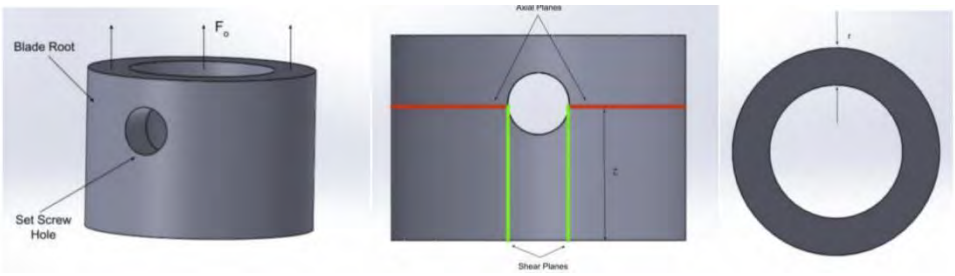

Figure 2-4 Root Load Analysis

The root designed for the blade was a female type root just as previous teams have done in recent years, and the pullout stress was also calculated analytically to determine the axial and shear stress at the set screw connecting the blade to the blade mount. For each of the conditions considered, the axial force (F_o) at the root was evaluated using the previous analysis. The maximum allowed stress of clear PLA material was determined to be around 41 MPa, based on a series of experiments conducted this year; color in the PLA actually makes the material weaker.

$$\sigma = \frac{KF_o}{A}$$

$$\tau = \frac{F_o}{4zt}$$

One part of this years report that has not been done was the inclusion of a foundation. The foundation team needs to know how much thrust force is pushing the turbine. Utilizing the following formula in excel we can evaluate the thrust on the turbine using equation 4-5.

$$T = -\int_{A0} \rho U_w \left(U_\infty - U_w\right) dA$$

Equation 2-5

2.5 Manufacturing

Once our design was completed the file was then exported as an STL file and imported into SOLIDWORKS where we could attach the root and with this assembly, we could save our completed blade design. After this we would utilize PrussaSlicer and Prussa 3D printers to physically make the blades. This manufacturing process is ideal because of the quickness and if there are any mistakes, the SOLIDWORKS file could be edited, and a new print could start and finished within a day.

3 Mechanical

3.1 Overview

The mechanical assembly of this year's wind turbine design is comprised of the variable pitch assembly, nacelle, tower, tail, and adapter stub. Most of the mechanical components were made from 6061 T6 Aluminum, due to its lightweight, strong mechanical properties, and easy manufacturability. Components such as the tailfin and tower were made from 3/32" steel sheet and carbon fiber tubing respectively. All components were manufactured in-house, being a combination of a Hass 5-axis CNC mill, lathe, manual mill, and plasma cam. Bearings, shaft collars, and all other fastening components that make up the mechanical assembly were outsourced from McMaster-Carr.

3.2 Variable Pitch Assembly

The design of the variable pitch was inspired from Cal Maritime's prior team's designs. The variable pitch assembly is comprised of 5 main components: the base hub, three blade mounts, three pitch levers, the pitch lever, and the actuator connection clips. The base hub is attached to the 3/8" stainless

steel shaft first by utilizing a tight transitional fit and secured by a through set screw. The three blade mounts are secured to the base hub using a shoulder screw, which allows the blade mounts to rotate against the bearing-like surface of the shoulder. The pitch lever then connects the blade mounts to the pitch driver and are also secured with shoulder screws, allowing for smooth radial movement between the linkages. The pitch driver is the component that moves axially along the shaft, driving all three pitch levers simultaneously and rotating the blade mounts. A 1 3/8" radial ball bearing is press fit onto the pitch driver and connected to two actuating connecting clips. The actuating connecting clips are secured using socket head screws, and do not experience radial movement. The function of the actuator clips is to interchange the linear force from the linear actuator to the pitch driver. All components in the variable pitch design rotate along with the shaft and rotor, while the actuator clips only experience linear movement across the shaft, as mentioned previously.

This year, the team has incorporated small iterative design changes in hopes to increase the structural integrity and pitching capabilities in this year's new performance tasks. The base hub now contains extruded spokes to position the blade mounts, allowing for greater depth of the shoulder screws that secure the blade mounts. The actuating clips now contain radial perimeters to decrease the overall surface area and material being used, without losing any structural integrity.

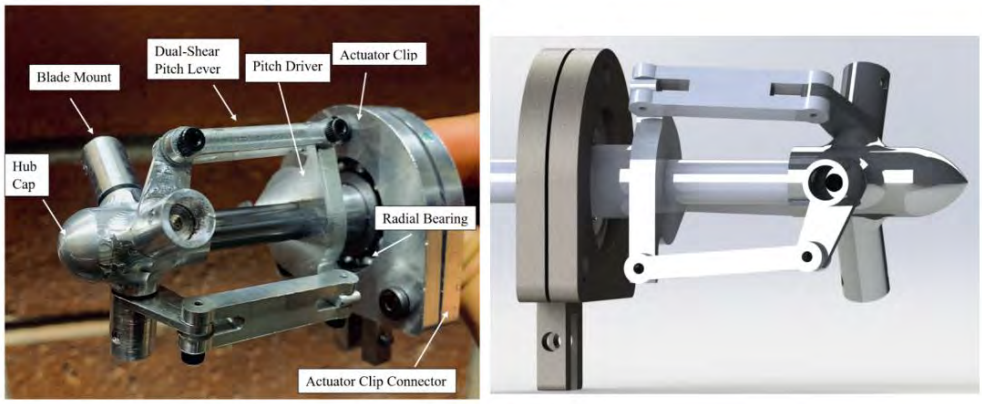

Figure 3-1 Variable Pitch Assembly: Prototype (Left) & SolidWorks (Right)

3.3 Free Body Diagram Analysis

To ensure smooth operations in our mechanical assembly, it was important to determine the correct size for the linear actuator. The most crucial property that the team needed to determine was the force capability of the actuator, as the actuator must be strong enough to overcome the incoming thrust of the wind. Several factors contribute to determining actuator force, such as air density, windspeed, rotational speed, blade geometry, blade angle, and the geometry of the whole pitch mechanism. Using these relations, we can create equations 5-1 and 5-2 to determine the necessary actuator force as a function of the blade angle by using free body diagram shown in Figure 3-2.

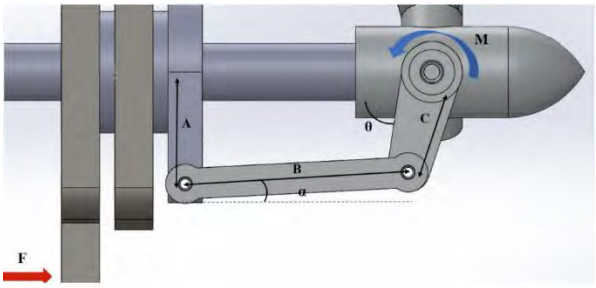

Figure 3-2 Free Body Diagram of Pitch Mechanism

$$F = \frac{3Mcos(\alpha)}{C\ sin(\alpha + \theta)}$$

Equation 3-1

$$M = \frac{1}{2} C_m \rho_{air} \int (U_{wind}^2 + (r\Omega)^2) c^2 dr$$

Equation 3-2

The pitch moment applied to each blade mount is calculated using Equation 4.3-2. The value was determined from blade load analysis, by implementing the geometric values of our airfoil and the worst-case wind speeds from the competition tasks of 22 m/s. From our analysis, we computed a maximum moment of 3.49 lbf-in, which we could then use to compute the force requirement from our linear actuator via Equation 4.3.1. It was determined that our greatest force to overcome was 24.7lbf.

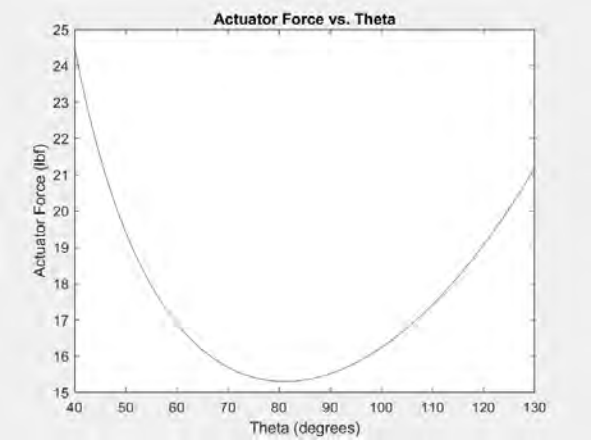

Figure 3-3 Actuator Force vs. Theta

From Figure 3-3, it can be observed that the actuator must cover a range of angles, however, it was only essential for our design that the variable pitch assembly have a 90-degree range. The blade mounts are initially positioned at a 45-degree angle (theta in Figure 3-2) which represent the full stop positioned (where braking will occur) and rotate to 135-degrees at the full run position (where maximum lift / rotation will occur). However, in order to cover a 90-degree range of rotation, it was essential that the actuator also contain enough stroke length. This property was also critical in choosing the right actuator. By using the geometric relations in Figure 3-2, we were able to calculate the maximum stroke length available in our linkage system is 0.95in. This analysis is critical as it is a characteristic needed when choosing the right actuator.

3.4 Actuator

From advice from Cal Maritime's 2020 and 2021's team, this year chose to use a linear actuator from Actuonix. The linear actuator this year's design will be using is a L12 Micro Linear Actuator with a 100:1 gear ratio and 30mm of stroke length (1.18 in). The 100:1 gear ratio provides 42N of force at a max speed of 13 mm/s. Other gearing options did not provide enough force or speed to securely control the position of our variable pitch mechanism.

3.5 Finite Element Analysis

To ensure no components in our variable pitch mechanism would fail due to the stresses in the system, finite element analysis was performed on the whole system to observe any potential failures. A full assembly analysis was performed on the variable pitch system at the worst-case, 22 m/s wind speeds. The results of the FEA is shown in Figure 4.4-1. It can be observed that the greatest stress the assembly will take is roughly 0.181 ksi, which gives us a factor of safety of 219, as the yield strength of 6061-T6 Aluminum is 39.8 ksi (refer to equation 3-3.

$$FS = \frac{Yield\ Stress}{Working\ Stress}$$

Equation 3-3

One of the major concerns observed from last year's design was the integrity of the shoulder screws holding the blade mounts onto the base hub. An analysis on the pull-out force of the threads was done to determine the safety of the shoulder-screws of the pitch system. In theory, the pull-out strength of a bolt is calculated by taking the product of the thread shear strength and the shear area. Using equations 4.5-2 and 4.5-3 provided from federal services of threads and standards, we calculated the pull-out strength of the 6-32 thread, alloy steel shoulder screw to be 1489lbf. From our blade load analysis, it was computed that the maximum centrifugal force the turbine would experience is 94lbf, if we set the maximum RPM of our rotor at 3000RPM. This gives us a factory of safety of 15, which proves that our blade mounts shall not pull apart from the hub any any working condition in the competition.

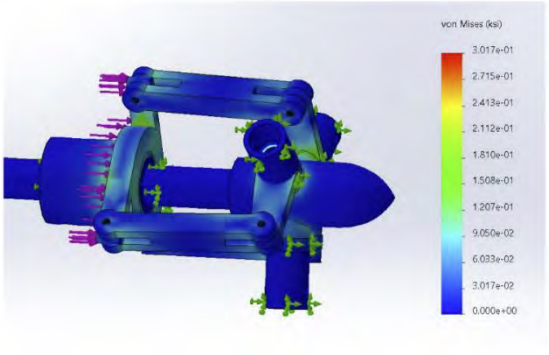

Figure 3-5 FEA of Variable Pitch Mechanism

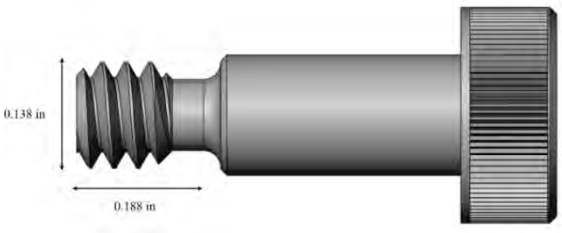

Figure 3-4 Blade Mount Screw Dimensions

$$PS = Shear\ strength\ (Weakest\ material) * Shear\ area$$

Equation 3-4 Pullout Strength of Threads

$$Shear\ area = \pi * n * L_e * K_n max\ (\frac{1}{2n} + 0.57735(E_s\ min - K_n max)$$

Equation 3-5 Shear Area of Threads

Where n is the number of threads/in, L_e is the fastener thread engagement, K_n max is the maximum minor diameter of the internal thread, and E_s min is the minimum pitch diameter of external thread.

3.6 Tower, Tailfin

This year's tower design has also been inspired from previous Cal Maritime team's designs. One exceptional change that the team has incorporated is the usage of carbon fiber tubing, as it is much lighter than aluminum yet more rigid. The tower design also allows for passive yaw, as it incorporates a radial bearing that connects to the base plate of the nacelle. To align the turbine in the direction of the wind, a 1/8" aluminum sheet tailfin will connect to the back of the nacelle. As passive yaw will not be a primary functionality of this year's competition, we chose to use aluminum sheet as it proved to be lightweight and rigid enough to provide enough turning moment on our turbine.

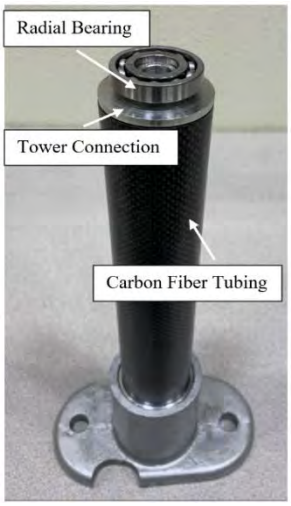

Figure 3-6 Tower Design

3.7 Mechanical Assembly Commissioning

The mechanical assembly, although complex in character, is rather simple in commissioning. To begin, the variable pitch system will be connected to a rigid coupler at in the Nacelle, that also connects to the rotor of our axial flux generator. The actuating mount is then connected to the nacelle, and bolted to the actuating clip connector on the variable pitch assembly. All components are contained within the nacelle, secured with ¼ - 20 steel bolts. The nacelle, with all components contained within, is then pressed onto

the outer diameter of the radial bearing on the tower. This connection is a tight, translational fit that contains a low tolerance to enhance the security of the connection. The tower is then secured to the base plate with M10 x 1.5 studs (as per rules and regulations), that is secured to the adapter stub on the foundational support.

3.8 Testing

From testing the variable pitch assembly, the team has seen great success in the variable pitch's ability to feather and run the blades. The first test computed was to determine the stroke percentage of the actuator needed to pitch the blades 90 degrees from full feather. From testing, it was determined that 78% of the actuator stroke fulfilled this requirement.

4 Foundation

4.1 Overview

Our foundation design is a combination of original ideas and outside inspirations. Because the offshore component is new to this year's competition, there are no references to previous teams' designs. Our final design consists of four anchors configured as a quadpod, with a central scribe piece that also acts as a monopile. The upper portion of the scribe consists of a square plate and a nominal 1.5" pipe. The lower portion is made up of steel rod and a baseplate. The anchors of the quadpod are angled in a way which minimizes a turning moment on the completed assembly. This is done by getting an approximate of where the loads are being impaired onto the structure from the turbine, particularly the thrust load, and then having the axis of the anchors virtually intersect at this point. The implication of this method is that the thrust force from the wind will be converted into tensile and compressive forces within the anchors.

4.2 Anchor and Scribe Components

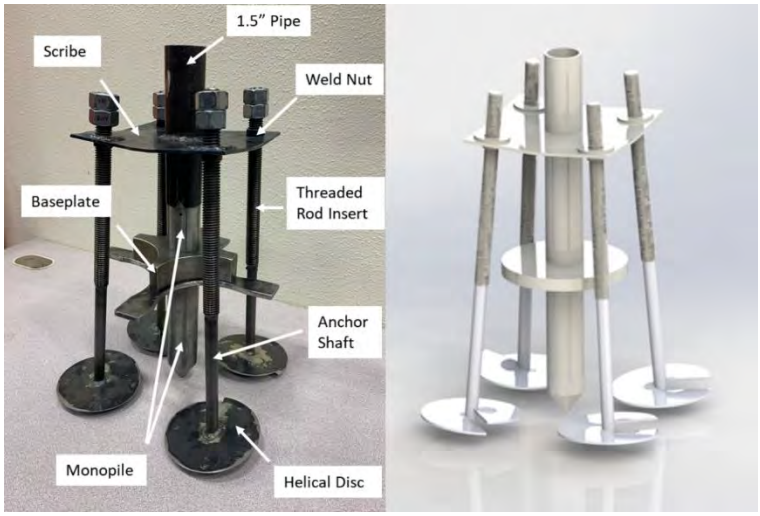

Figure 4-1 Foundation Assembly: Final Version (Left) & SolidWorks (Right)

As per the competition rules, all components are made of steel and fastened together by threads, spring pins, TIG welds, or a combination of these methods. Each of the four anchors consists of a machined tip, tubing for the anchor shaft, plasma cut helical disc, spring pins, and a modified 5/8"-11 threaded rod. The machined tips were turned to size from steel rod using a lathe. These tips are then pinned into the nominal 0.5" steel tubing, which makes up the lower part of the anchor's shaft. The disc, after being plasma cut from a steel sheet and bent into a helix, is TIG welded onto this tube just above the end where the tip is secured. Threaded rod is cut to size, turned down on one end, and inserted into the

tube with a spring pin securing it. The rods are also welded to the tube, making for a more secure connection that ensures structural support during the high torque of installation. All four of our anchors can be seen in Figure 5.1.1. In this configuration, they are deployed to their proper lengths via the threads and fit within the 25cm square area defined in the rules. The method to which we arrived at our dimensions will be detailed in section 5.3.

Inspiration for our anchor design came from Ojjo Inc. This San Rafael based company designs, constructs, and installs foundation trusses for solar farms. Our team was able to visit one of their locations through a connection our advisor has, and we were able to gain firsthand exposure to some of their technologies. Through testing of our own, we confirmed that a helical anchor performs well in loose soil when it comes to pushing or pulling forces. Other common designs that we researched were not feasible or sturdy enough to work in this competition's scenario. For example, the suction bucket method would require materials other than ferrous ones to work properly. Also, when we tested how a lone monopile would behave in the designated sand, a monopile-like structure was subject to tipping with the slightest forces. Creating our own sand and water enclosure early on gave us an asset for gauging what sort of structure would be required. Once we started constructing different helical anchors, we were able to gather data on how much force different designs could take. This data is presented and elaborated on in section 5.4.

The scribe and monopile consists of a plasma cut steel plate, nominal 1.5" pipe, steel rod of a similar size, four 5/8-11 weld nuts, and a 1" thick steel disc stacked upon a wider plasma cut steel plate. The scribe piece, made of 1/8" steel plate, was specifically plasma cut to house the four weld nuts and the center pipe. The bends on each corner of the plate were achieved using a vice and mallet. Though we were initially concerned about the precision of this method, the use of an angle protractor confirmed that we were achieving the desired angle. Our method on choosing this angle will be detailed in section 5.4. The four weld nuts were then placed in their slots and TIG welded to the square scribe. This was done after the bending of the corners to avoid breaking the welds. At this point, the scribe was welded onto the 1.5" pipe that serves as the connector to the stub assembly. Specific care was taken in measuring the length of pipe that is above the scribe piece to ensure that space was available, as per rule requirements.

Figure 4-2 Leveling the Scribe - TIG Welding

The monopile consists of two machined pieces which compress the baseplates between them via a threaded connection. The top piece was spring pinned into the 1.5" pipe to stay in place. A female thread on its underside connects with a male threaded section on the topside of the pointed monopile component. As shown in Figure 5.1.1, the baseplate is in between these two components of the monopile and secured by the torque applied on the threads. The baseplate has a different design than that of the SolidWorks model because of a recent modification to the design. The helical anchors need to begin in a position that is higher than the tip of the monopile for ease of

installation. We adapted our 1” disc baseplate into a cross-like shape to provide this clearance and added an additional 1/4" plate to provide more surface area. This cut down on our total weight and added more contact with the surface of the sand. Having the baseplate on the surface of the sand and our scribe just below the water line helps position our assembly correctly. The goal of the different levels of our foundation is to clearly define where it fits within constraints.

Figure 4-3 First Prototype - Tripod

Those of our team working on the foundation had to develop skills that were needed to complete the required manufacturing. This included much manual machining on lathes and mills, some of which required specific angling and threading. Additionally, plasma cutting using CAM software was critical to manufacture components of our foundation. To fasten our pieces together, TIG welding proved to be the best option. Through repeated exercise of these skills, we were able to complete a final assembly.

At first, we were using a flat head drive to install the anchors into the sand. This utilized a slit in the top of the threaded rods, but this method proved to be inadequate. Instead, by using a double nut configuration at the top of each anchor, we can transfer a substantial amount of torque to the legs via a socket wrench and impact driver. This greatly reduces our installation time and required effort. More detail on our process, including the packing of the sand, will be detailed in section 5.4.

Our first complete prototype incorporated a tripod design, but due to size constraints and force testing, we shifted our efforts to a quadpod design. However, to conserve our resources and time, we manufactured our components in a way which made them modular. For example, the threaded rod and tip of our anchors were made to be removable. Therefore, these parts did not need to be machined again when the disc size changed. Also, the monopile structure was only pinned into the bottom of the piping welded to the scribe. Yet, it was sturdy and still able to be reused with our final quadpod design. In Figure 5.2.2, our first prototype can be seen with the same parts we were able to reuse in our final design.

4.3 Dimensioning Methods and Force Analysis

As shown in figure 4.3.1, we tested various disk sizes for the legs of our foundation. We hypothesized that the larger the disk, the more pull force required to move the legs in the sand. To test this hypothesis, we used excess rod material and welded several different size disks to the cut rods. The disks were welded as close to the bottom of each rod as possible to maximize the depth each disk is driven into the sand. Each test rod was marked with tape at 15cm to ensure the testing did not exceed competition rules. To maximize the required amount of pull force to move each leg, each leg was buried the full 15cm and the sand was packed around each leg before testing occurred. To test the legs, we attached a strain gage to the rod and recorded the force required to move each leg vertically. We repeated this test ten times for each leg and took an average of our results.

Figure 4-4 Anchor Tension Testing

We also tested the having multiple disks on the legs. We hypothesized that having more disks would increase the amount of pull force required. However, we found a journal [5] that did similar testing on helical anchors for offshore foundations. The article stated that having multiple disks is not effective if the distance between them is too shallow. The article gave a formula to calculate the distance required

between two disks for them to be effective: S = DP*Number of Disks (where s = the distance between disks, and DP = the disk size). Using the previous formula, we determined that the competition sand depth is too shallow for multiple disks to be effective. The article also went into great detail about how the pitch of each disk effects the installation torque. Due to the small size of the disks, we were not concerned with the pitch as we had no difficulties installing each anchor.

During our tension testing, we noticed that the anchors would fail two ways: either the entire column of sand above the disk would shear upward with the disk or the sand would be pushed upward with the disk. This is consistent with the findings in [5]. We did not conduct any detailed compression loading on the disks as we found that the disks could significantly handle more force in compression than in tension. A single 2.5" disk on a leg was able to take over 200 newtons of force before moving.

Table 4-2 Disk Size Testing

Disk Testing					
2.5 inch Diameter		4 inch Diameter		5 inch Diamter	
Test #	Pull Force	Test #	Pull Force	Test #	Pull Force
-	Newtons	-	Newtons	-	Newtons
1	40	1	66	1	84
2	38	2	68	2	86
3	37	3	76	3	86
4	38	4	74	4	68
5	38	5	70	5	69
6	34	6	66	6	65
7	33	7	62	7	69
8	36	8	55	8	66
9	34	9	60	9	59
10	35	10	58	10	65
Average	36.3	Average	65.5	Average	71.7

Table 4-1 Number of Disks Testing

Number of Disks Testing			
2.5 & 1.25 inch		2.5 inch	
Test #	Pull Force	Test #	Pull Force
-	Newtons	-	Newtons
1	36	1	40
2	37	2	38
3	36	3	37
4	33	4	38
5	37	5	38
6	29	6	34
7	32	7	33
8	36	8	36
9	36	9	34
10	32	10	35
Average	34.4	Average	36.3

As shown in our testing results above, our hypothesis was confirmed that larger disks have a significant advantage in resisting movement. Furthermore, it was confirmed that our legs are too short for multiple helical disks to be effective, as noted in [5]. The pull force required was for multiple disks compared to a single disk was relatively the same. Therefore, we decided to move forward with a single disk design.

For our legs, we chose to use 4-inch disks. Even though we learned that larger disks had more resistance to movement, we found that the angle between the legs and turbine tower had a significant effect on the amount of force exerted on each leg. The larger the angle, the less force exerted on each leg. This theory is proved in our MATLAB calculations below. Using 4-inch disks, the maximum angle we could use to stay within the 25cm-by-25cm competition rule was 5 degrees. We calculated this using the geometry in the figures below. Each disk was placed directly in the corner ($\beta = 45°$) of the 25cm-by-25cm area to maximize the angle, α, between the tower and each individual leg.

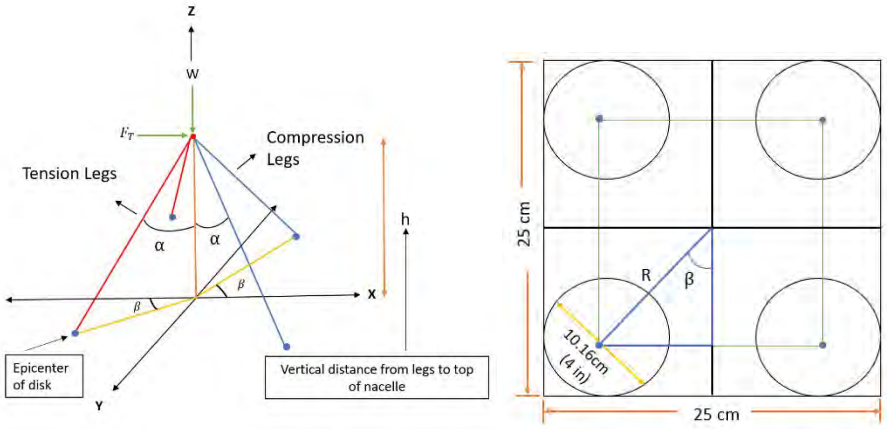

Figure 4-5 Free Body Diagram of Analysis and Disk Set Up

A MATLAB analysis was computed to estimate the rough expected forces in each leg from a computed worst case thrust force on the turbine and estimated weight of the nacelle. The thrust calculation is explained in section 2.4 of this report. The analysis assumes that all forces act at the top of the turbine and centerline. The forces are then distributed through the four legs. The front legs absorb the tensile forces on the structure and the back legs absorb the compressive forces on the structure. The following static equilibrium equations and MATLAB script were computed using the free body diagram above.

$$\sum F_x = 0 \text{ (Due to Symmetry)}$$

$$\sum F_y = F_T - 2T*\text{Sin}(\alpha) * \text{Cos}(\beta) - 2C * Sin(\alpha)*\text{Cos}(\beta) = 0$$

$$\sum F_z = W + 2T*\text{Cos}(\alpha) * -2C * Cos(\alpha) = 0$$

```
%William Laurent and Aaron Breitinger
%CWC Foundation Optimization
%4/13/2022
clear; close; clc;
FT = 47;                %Worst Case Thrust Force (Newtons)
W = 10*9.81;            %Estimated Nacell Weight (Newtons)
beta = 45;              %Angle of legs relative to sand (Degrees)

ii = 1;                 %counter
%loop to calculate disk sizes
for D_R = 0.5:0.25:2.5 %disk radius
    R = (sqrt((12.5-(D_R*2.54))^2 + (12.5-(D_R*2.54))^2))/100; %meters
    h = 1.15; %meters
    alpha = atand(R/h);
    x = [2*sind(alpha)*cosd(beta),2*sind(alpha)*cosd(beta);-2*cosd(alpha),2*cosd(alpha)];
    y = [FT;W];
    A = x\y;
    T(ii) = A(1,1); %Tension Values
    C(ii) = A(2,1); %Compression Values
    ii = ii + 1;
end
x = 0.5:0.25:2.5;
subplot(2,1,1)
plot(x*2,T),title('Tension Force vs. Disk Diameter');xlabel('Disk Diameter (inches)');ylabel('Tension (netwons)');
subplot(2,1,2)
plot(x*2,C),title('Compression Force vs. Disk Diamter');xlabel('Disk Diameter (inches)');ylabel('Compression (newtons)');
```

Figure 4-6 Static Equilibrium Equations and MATLAB Analysis

The MATLAB code functioned to show the force distribution in each leg, given the disk size. As the size of the disk increases, alpha (the angle between the tower and legs) must decrease to stay within the 25cm-by-25cm competition area rule. From our results we choose to use 4-inch disks which corelates to an alpha of 5 degrees. We choose the 4inch disks as we noted from Figure 4.34 that the tension and compression forces are drastically reduced at the resulting alpha for this disk size. Furthermore, the 4-inch disks are almost twice as resistant to tension as the 2.5-inch disks, while the force reduction at an angle with 2.5-inch disks does not result in as significant of a force reduction. The results of the code showed that each tension leg needs to absorb 166 newtons and each

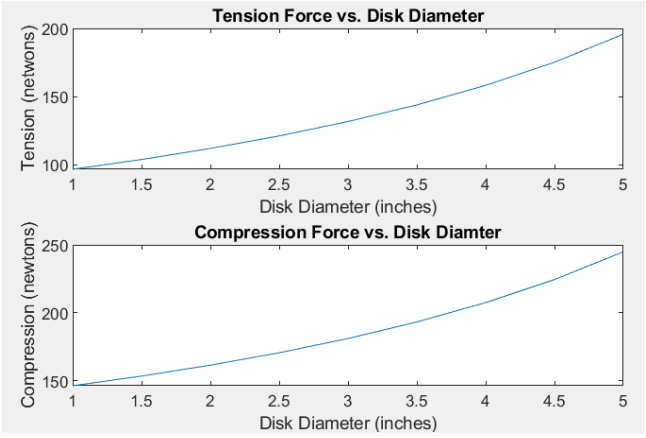

Figure 4-7 MATLAB Angle Analysis

compression leg needs to absorb 215 newtons at an angle (alpha) of 5 degrees. From our pull tests we knew that each 4-inch disk leg was able to absorb about 65 newtons when vertically pulled. Since this is not enough to overcome the thrust and weight forces, we decided to incorporate a monopile and baseplate to our assembly to help absorb the remaining forces. We hypothesized the monopile would add more stability because of the weight addition below the sand. The baseplate has a large surface area that covers the top of the sand and a weight addition. We hypothesized that this increase in surface area and weight would add more stability to the foundation.

Figure 4-8 Foundation Assembly Testing

To test if the baseplate and monopile additions would be enough to absorb the forces, we tested the entire assembly in our testing tank. We would assemble the foundation following the steps stated in section 6.4 of this report. We then would insert a rod into the tube of the foundation. The rod was cut to length so it would be roughly the length of the nacelle. We then would attach a strain gage to the foundation and pull in the direction of the thrust force. The amount of thrust force required to move the turbine was recorded. Our test did not incorporate a downward weight force like the MATLAB script. This adds a factor of safety to our analysis as we found that the addition of weight reduces the amount of tensile and compressive forces in the structure.

In our testing we found that the tension legs would fail before the compression legs as expected. We got an average of 49 newtons required to move the structure. This means that our foundation will be able to handle the worst case thrust force of 47 newtons. The computation of the thrust force is explained in section 2.2, during competition and indicates that our design is a success. In our testing we recorded the thrust force that would move the turbine and not the force that would cause complete failure. We found that thrust forces below 70 newtons would move the turbine, but when the load was removed the foundation would settle back into its installation position. This also adds a factor of safety to our analysis as we believe the foundation will be able to take greater thrust forces than 47 newtons and not completely fail.

Table 4-3 Foundation Testing Results

Foundation Testing			
Test #	**Installation Time**	**Failure Force**	**comments**
-	**Minutes, Seconds**	**Newtons**	**-**
1	4 min, 32 Sec	38	no packing
2	5min, 34 Sec	42	no packing
3	7 min, 28 Sec	51	packing
4	9 min, 29 Sec	45	packing
5	10 min, 38 Sec	53	packing
6	8 min, 33 Sec	48	packing
7	8 min, 27 Sec	54	packing
8	4 min, 55 Sec	48	packing
9	6 min, 42 sec	46	packing
10	6 min, 45 sec	43	packing
Average	7 min, 15 sec	49	packed only

4.4 Assembly Commissioning Checklist

Before installing the foundation into the enclosure, it must first be properly assembled. The baseplate, which must be torqued on squarely to the scribe, is compressed between the monopile pieces. Due to a slight variation in the angle of each anchor, they must be matched to the corresponding weld nut. Also, the shape of each disc is slightly different due to the imperfect method of bending them. If care is not taken in these areas, there may be collisions between the anchors and the baseplate during installation. To keep track of which anchor goes where, a matching letter is scribed into each disk that matches a similarly scribed letter in the baseplate.

Figure 4-9 Impact Driving the Anchors

Once the scribe, anchors, and monopile are secured in the correct fashion, two nuts are threaded onto the top of each anchor. The lower one is held while the upper one is tightened down onto it. This allows for the driving of the legs using hex drives on a wrench or impact driver. For additional adaptability, the tops of the anchors also have a slot that can be driven with a flathead tool. Like mentioned before, the flathead is an inadequate driving tool when in the sand. However, it is useful to have so the anchors can more easily be put in the retracted position before installation.

Next, the entire foundation is placed into the enclosure. With some slight movement in a circular motion, the monopile drives into the sand until the baseplate makes contact. This can be felt by the installer. At this point, the scribe should be just under the water line and checked with a bubble level. Using a socket wrench, the anchors are evenly rotated into the sand for a few turns. By using the manual wrench at first, we avoid damage that could be caused by the high torque of the impact driver if there was accidental contact with the baseplate. Also, the sand may be disrupted too much if the anchors are initially driven at high speed. The impact driver is then used to drive each anchor deep into the sand. During this process, a pipe that fits into the top pipe of the foundation is used to help hold the entire assembly in place. Just before the nuts contact the scribe, we switch back to using the socket wrench. Again, this allows for more control that is critical to finishing the installation. Each anchor is carefully turned into their fully deployed position.

Figure 4-10 Packing the Sand

Lastly, the sand is packed around the anchors. To avoid touching the water, just like in the rest of the process, a tool is used to reach down into the enclosure. This tool is simply a pipe connected to a wide disc that fits around the anchor shaft. This allows for effective packing close to the sand that is absorbing a majority of the load. The competition stub is then attached to the top pipe.

5 Generator

5.1 Overview

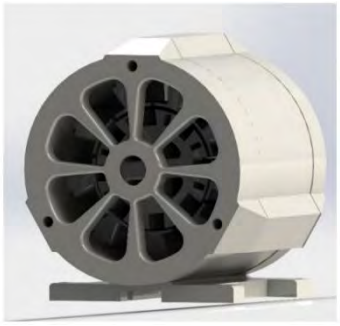

Figure 5-1 Generator Assembly

Both the 2020 & 2021 Cal Maritime teams came up with the idea of designing and fabricating their own custom generator. We also believe that creating a custom generator would have lots of advantages and would result in an overall better performance. Purchasing a generator removes the customization factor, therefore many problems arise such as the lack of power production at low wind speeds and the inability to remit cogging torque. Cogging torque is the amount of opposing torque produced between the magnets and any ferrous material. Our team members have taken an Electrical Machinery course where we are required to create our own generators from scratch. This course gave us all the tools and experience to create a custom generator for the Collegiate Wind Competition. Fabricating the generator allowed a minimal amount of internal power loss, improved cut-in speeds, and provided greater power generation at high wind speeds. Other advantages of a custom generator are the reductions of cogging torque, cost-effectiveness, optimization of the turbine's power curve, and the ability to create a generator with our own desired characteristics.

The two generator designs that were researched were radial and axial flux designs. Both configurations were fabricated using a 3D printer and were tested in our home wind tunnel. Each design was a great option, but we were more comfortable with the radial flux design because of previous experience using that arrangement. The radial flux design allowed the windings on the teeth to use a thicker wire gauge which minimized the number of windings to wrap around each tooth. Using fewer wraps on the teeth permitted the maximum possible effect of the flux density.

5.2 Theory & Coil Estimation

The underlying principle behind our generator is based on Faraday's law, which states that when a changing magnetic flux passes through a loop of wire, a voltage will be induced. Shown by equation 6.2.1, that voltage will generate a current to oppose the incoming magnetic flux, hence the negative sign. This is an incredibly important characteristic of Faraday's law which drove the need to build homemade generators – since cored stators have more efficient magnetic circuits and thus has a greater opposing magnetic field. This opposing magnetic field produces what's known as cogging torque, which is a very undesirable characteristic for start-up speed.

$$V_{ind} = -N\frac{d\phi}{dt} \quad \textit{Equation 5-1}$$

$$V_{DC} = \frac{3*\sqrt{3}*12NA\omega k_w B_{max}}{\pi} \quad \textit{Equation 5-2}$$

We can use Faraday's law to characterize the DC voltage output induced by our eight pole, nine coil generator – where N is the number of wraps per coil, ω is our angular velocity in rad/s, B_{max} is the maximum observed magnetic field on the face of the rotor, A is the cross sectional area of our coils, and k_w is the winding factor. Knowing that we are constrained by 48V, estimate from prior generator builds that our

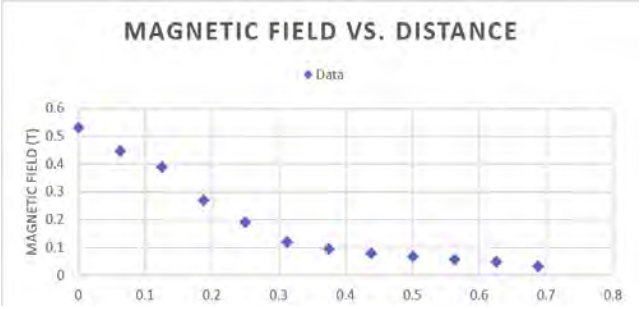

Figure 5-2 Gauss Meter Test Results (Halbach rotor)

maximum angular velocity up until rated wind speed does not exceed 3000RPM, designed our coils to match a $3" \times \frac{3}{8}" \times \frac{3}{8}"$ magnet, and deduced that our winding factor is about 0.94521 based on our pole & coil arrangement. Therefore, we needed to determine the magnetic field experienced by our field to estimate the number of wraps per coil to meet our criteria.

Once the rotor was fully assembled with the Halbach array, we proceeded to conservatively estimate the magnetic field that the coils are experiencing by recording the flux density found at the center of the magnet at a given vertical distance, given in 1/16" increments. With the plot in **Error! Reference source not found.**, taking a weighted average from 0.125" (distance from our rotor surface to first coil) to 0.625" (our stator caps are ½" long), we calculated a value of 0.122T. With all our parameters known, we estimated that the number of coils needed to achieve 48V on our first iteration was roughly 90 wraps.

5.3 Radial Flux Design

Our radial flux generator is composed of nine stationary teeth, press-fitted onto the stator, that hold the coil windings. The teeth are oriented in such a way that the windings wrapped around it will generate magnetic flux radially, perpendicular to the shaft when the rotor spins. In order to maximize the magnetic flux that can be generated, the clearance between the rotor and the teeth is very minimal at 1/16 of an inch. The rotor has eight main permanent magnets fixed onto it that are in a traditional alternating pattern and eight secondary magnets placed in between each main magnet. The secondary set of magnets are oriented by 90 degrees from the previous magnet, ultimately creating the Halbach Array. The Halbach Array configuration is very advantageous as it concentrates the magnetic field onto one side of the magnets, creating a strong side, in exchange for a weak magnetic field on the other side of the magnets. This means that a stronger magnetic field can be emphasized outwards towards the windings, while leaving the sides facing the shaft weaker. Overall, this Halbach Array maximizes the generator's ability to produce power, without having to use a larger design.

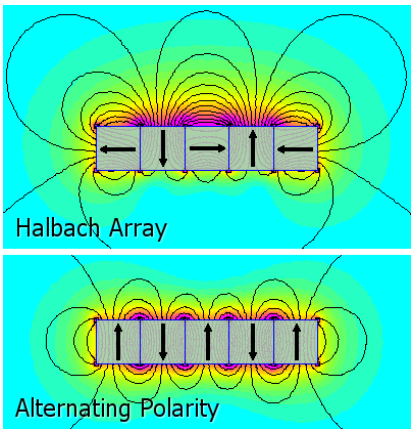

Figure 5.3.1 Magnet Configuration [3]

To further maximize power production, our team chose to wire our generator in a wye-configuration instead of a delta configuration since our results from previous generator projects showed that a wye-configured generators produced more power when tested in our home wind tunnel. A wye configured generator will have a total of four wires: three hot wires (one for every phase) and one grounding wire connected to the neutral point that connects the phases. The produced three-phase alternating current is then converted to DC through a rectifier, which we can then easily connect to our loads.

5.4 Assembly Checklist

Our generator follows a modular, compact philosophy. A modular generator design allows us to service different parts in case of failure or mishaps during testing. In addition, having modular, small parts allows us to reprint parts individually, if needed, as opposed to reprinting the whole assembly. This also saves lots of printing time. This was especially key for the generator teeth in which the copper coils are wrapped around. It was convenient to print different sets of teeth so that the generator performance

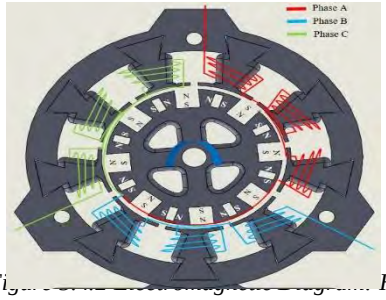

Figure 5.3.2 Electromagnetic Diagram: Halbach Array & Wye Configuration [3]

could be tested with different wire gauges and the number of coil wraps, as opposed to unwrapping then rewrapping one set of teeth.

With our generator design, the assembly process can be done easily. The rotor has embedded slots for the arrangement of the magnets. A layer of epoxy was applied to each slot before placing the magnets to maximize the security of the magnets onto the rotor, while spinning. The shaft is a press-fit insertion into the rotor and a flange was added to minimize the possibility of slip. Journal bearings were also added along the shaft to support the radial loads on the shaft. Two thrust bearings were used to support the axial loads. One of the thrust bearings is physically on the generator end cap, while the other was placed on the nacelle. Once the teeth were wrapped with the correct number of coil windings they were placed in their press-fit dove-tail housings. At this point, the wire ends were soldered in the wye configuration, wrapped in heat shrink, and placed in the groove made on the end cap which serves to house the wires in an organized manner. The entire assembly was secured with three aluminum bolts and 6 nuts that fastened all the generator components together.

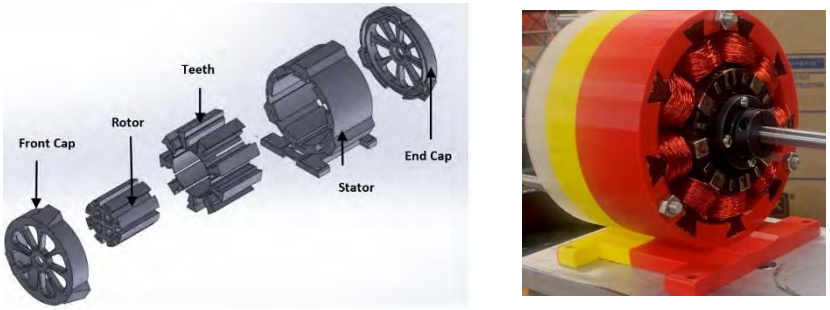

Figure 5.4.1 Generator Assembly: SolidWorks (Left) & Prototype (Right)

5.5 Rotor Safety

Our rotor is the only component of the generator assembly that is subject to any significant loading; since we are expected to experience 20+ m/s of wind speeds, it is critical that the rotor is rigid enough to withstand the significant centrifugal loads that come with it. Having to consider the centrifugal loads that the epoxied magnets exerted on the rotor, not to mention the PLA's own centrifugal loading, an FEA analysis using Von Mises static failure theory was done to determine if the rotor would fail or not. The result of our test, shown in shows that our rotor is able to withstand the loads that may be introduced by a load disconnect at high wind speeds. Considering our maximum Von Mises stress and the yield strength, we achieve a factor of safety of 15.

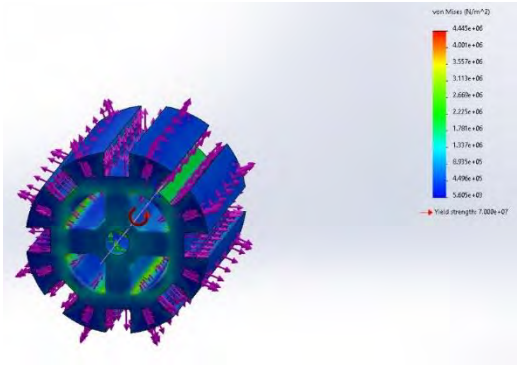

Figure 5-3 Rotor under load at 7000RPM

6 Electronics and Controls

6.1 Electronic Systems

For this year's electronics system we set out to improve upon the 2021 electronics systems design. The 2021 Electronics system failed during the point of common connection (PCC) disconnect task, being that it was unable to fully feather the turbine blades under just generator power when the load was

disconnected. To combat this, this year we aimed to increase the rate of feathering for our actuation system and extend the run time of the turbine side control system during the PCC disconnect task. Our Electronics system is split into 2 subsystems meant for either the Turbine Side, or the Load Side of the PCC.

6.2 Turbine Side

This year our generator will be producing 48v DC after rectification of the AC Voltage from the generator. The figure to the right is a diagram of the system being described. The DC Voltage from the connects to our Turbine Side Control board. The DC voltage is run in parallel with 2 3900 µF capacitors; these extend run time to our microcontroller, and pitch actuator, in addition to providing smoothing for out DC output from the rectifier. The extended run time increases the likelihood that our turbine feathers completely during the PCC disconnect task. The output DV Voltage is regulated then to 5V, and 6V respectively by DC-DC converters. The 5V supply is used to power the Teensy 4.0 Microcontroller. The 6V supply is used to power the linear actuator on the pitch mechanism. The reasoning for having the 2 supplies rather than just the one 5V for both systems was we found that there was a measurable performance advantage in terms of speed for the linear actuator when it was run at 6V rather than 5V. Additionally we found that the regulator we had used for the 2021 Turbine Control system capped out at supplying 460mA with a voltage input of 48V, this was less than the expected current draw at operation for both the microcontroller and the linear actuator. Thus, by splitting the 2 loads to their respective regulators we ensured that they would both have sufficient power. Our emergency shutdown switch is also located on our Turbine Control Board. On the output end of our Turbine Side control board, we are employing a pull-down voltage divider to pull supply voltage at 48V down to 3V to measure voltage using the microcontroller's analog read ports. Also measured on the output end of the board is current, we are utilizing an INA169 high side current sensor rated for 2.75-60V. The current and voltage measurements are used in tandem to control the pitch actuator via the Teensy micro controller allowing us to control for voltage and power, the specifics of which is discussed later in the report. The negative side, or common as indicated in the diagram, is the earth ground of the system, the entire circuit is tied to the earth ground to prevent overvoltage of the PCC.

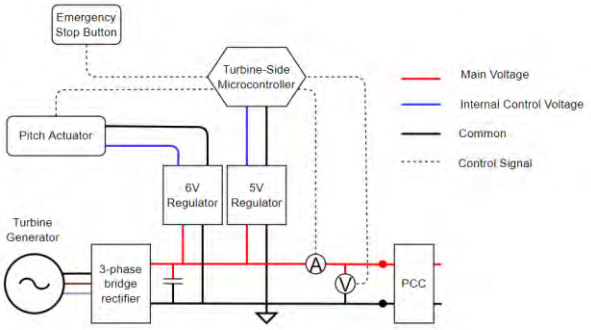

Figure 6-1: Turbine Side One-Line Diagram

6.2.1 Emergency Stop Circuit

The emergency stop circuit pictured to the right takes 3.3V out from the Teensy Microcontroller and runs it through the emergency stop which is normally closed. When opened the circuit stops supplying voltage to an analog input on the Teensy. The Teensy generates a control response which is discussed further in section 6.2.1

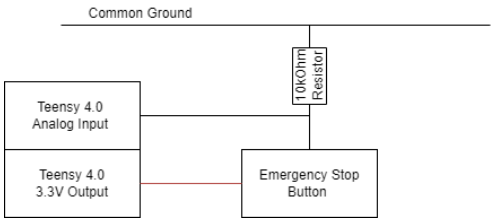

Figure 6-3 Emergency Stop Circuit

6.2.2 Voltage Sense Voltage Divider

To measure the voltage on main, this year we will be using a pulldown voltage divider to pull a 48V nominal signal down to 3 Volts. The circuit is pictured to the right.

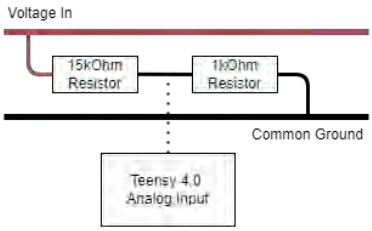

Figure 6-4 Voltage Sense Circuit

6.3 Load Side

The load side electronics system connects to the PCC and serves as a switching circuit between a 6V battery and our fixed resistive load. The load side like the turbine side control board utilizes a pull-down voltage divider to measure voltage from the PCC, and an INA169 Current sensor to measure the current. The Teensy microcontroller decides whether to power a relay that switches the circuits connection to either the battery or fixed resistive load. The battery serves to power the Turbine Side microcontroller when the generator does not provide sufficient power due to braking or safety shutdown conditions. The 6V battery through an additional 5V regulator will provide power for the Teensy 4.0 Microcontroller. The microcontroller on the load side reads current and voltage and controls the relay.

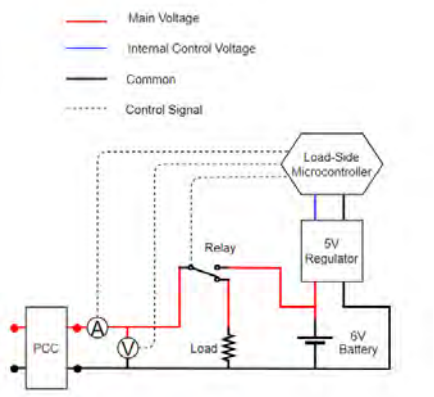

Figure 6-5: Load Side One Line Diagram

6.3.1 Detailed Relay Circuit

Our relay circuit is summarized by [insert relay circuit here]. It is powered by our 6V battery and switched on via our TIP102 MOSFET, with a flyback diode to prevent current discontinuities. For conventional logic, we will use a normally closed relay to the load – that way an activated relay will leave the load resistor open and allow for a path from the 6V battery to the PCC.

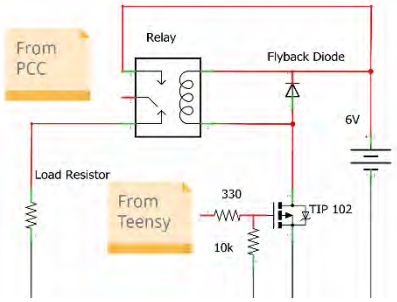

Figure 6-6: Relay circuit

6.3.2 Construction/Manufacture

Both control boards were constructed on perfboards utilizing soldered wire connections to build the circuit. Inputs and outputs to/from external sources are conducted using screw terminals. The INA169 current sensor is on its own break out board and has not been soldered onto the either control board instead having soldered connections and a separate mounting assembly.

6.4 Safety Task Control Schemes

6.4.1 Emergency Stop Task

Our first safety task is to shut down operations of our turbine in case of an emergency. For the turbine side microcontroller, its only task is to sense the button being pressed, and consequently pitch the blades to full feather position. The load side microcontroller senses a loss in voltage and current at a particular threshold, and switches on our MOSFET-driven relay from the load to our 6V supply to maintain power to our turbine side microcontroller. A good threshold for our voltage would be 5-9V, since that is what is needed to power our microcontroller; whatever our current turns out to be at that voltage would also make for an acceptable threshold.

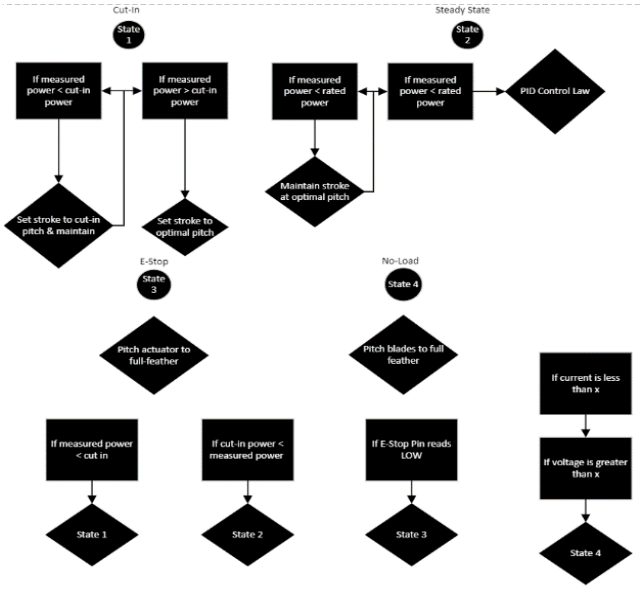

Figure 6-8: Turbine side logic

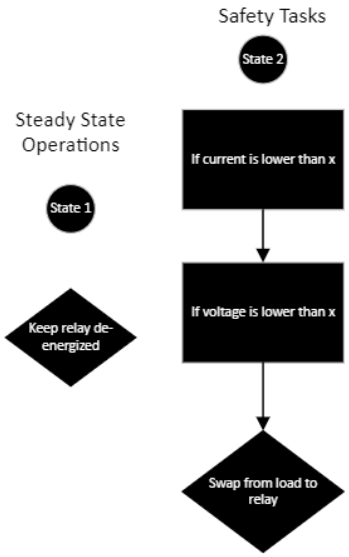

Figure 6-7: Load Side Logic

6.4.2 Load Disconnect Task

For our load disconnect task, we must be able to successfully shut down our turbine in the event of a load disconnect from the PCC. If a load disconnect does occur, there will be no current through our system and thus no mechanical load – leading to our turbine spinning faster and inducing more voltage than usual. It makes sense to set our voltage threshold at 50V, since we are constrained below 48V anyway, and our current threshold nearing zero since our current sensor will have an open circuit. Our load side logic should be the same as that of the E-Stop; once the load connects again, the 6V battery will power our turbine side microcontroller to return the actuator stroke to steady state operations

6.5 Actuator-Blade Plant Closed Loop Control

The goal with this system is to utilize our variable pitching system to regulate our power output at 11m/s. Beyond that wind speed, there is no benefit to increasing our power output scoring-wise and only introduces more centrifugal loads on our rotor. Since we are sensing voltage and current in our turbine side circuit for other purposes, it makes sense to regulate power and, inadvertently, the speed using variable pitching to maintain steady state operations as if the turbine was experiencing 11m/s wind speeds. **Error! Reference source not found.** summarizes the control scheme of our actuator-blade system.

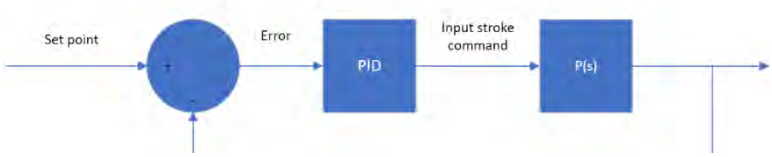

Figure 6-9: E-Stop State Diagram

Figure 6-10: Actuator-Blade Plant Block Diagram

Table 6-1 System Identification Parameters

6.5.1 Open Loop Testing

The actuator-blade plant is the overall dynamic system encompassing the variable pitching mechanism used for our turbine, which takes a stroke command from 0-100% as a step function input and outputs power. In order to effectively control this system, a model is necessary to understand how an actuator stroke command causes the power to respond. The dynamics behind this system is complicated and involves the motion of our actuator, the aerodynamics of our blades, the inertia of our rotor, etc.

Actuator-Blade Transfer Function Parameters	Values	Units
y_F	-7.70	W
$u(t)$	-15	%
σ	1.65	N.A.
K_{static}	0.514	W/%

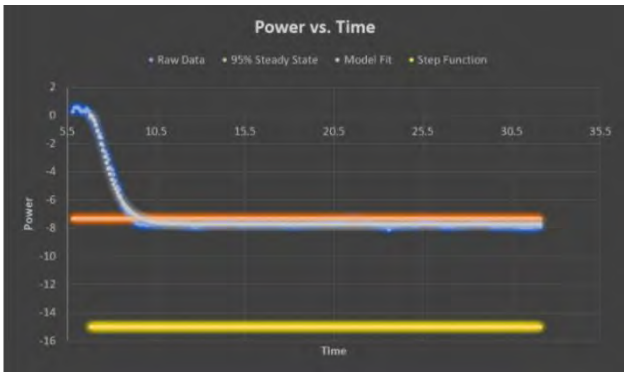

Figure 6-11: Open-loop testing results

Rather than using laws of physics, we modeled our system as a black box model: our input is a stroke command, and our output is electrical power produced. To do this test, we kept wind speed constant at $7\frac{m}{s}$ and load resistance constant at 192Ω. Using a microcontroller to manually set our stroke length, we obtained data on how our power output as a function of time responds to an actuator command. It is observed that the response closely resembles a 2nd order critically damped system – the relevant parameters are provided in **Error! Reference source not found.**. Using this model will help us make educated decisions about our PID gains.

6.5.2 Closed Loop Control State Diagram

Error! Reference source not found. summarizes the logic behind our control law for regular turbine operation. When starting up, our optimal blade pitch is usually not the best way to go; a more aggressive pitch makes for easier start up. Once the turbine is cut in, setting the pitch to full run will increase power production dramatically. Whatever we produce at 11m/s will be considered our rated power, and it will no longer be advantageous to produce any more power – which is when the PID controller activates.

6.6 Optimizing Resistance

As per the competition rules, we are only able to use passive resistance for our load. For each wind speed, there is a resistance that will produce optimal power. **Error! Reference source not found.** shows initial testing results for optimizing load (going beyond 8m/s would compromise our PCC), and with this we can project a load curve to fit the peaks we want to hit.

Figure 6-1: Turbine operation state diagram

7 Bibliography

[1] CWC 2021, Barrons, T. B., Dixhorn, J. V. D., Hesse, R. H., Hooper, G. H., Morgenstein, M. M., & Rosenberger, A. R. (2021, May). U.S. Department of Energy Collegiate Wind Competition: Technical Design Report 2021. CSU Maritime Academy.

[2] CWC 2020, Brown, T., Eagle, F., Kruschke, S., Jo, C., Nguyen, A., Skarin,J., Smith, M.,Sprague, T., Rodriguez, S., Wang, J., Vargas, A., (2020, May). U.S Department of Energy Collegiate Wind Competition: Technical Design Report 2020. CSU Maritime Academy

[3] Kjmagnetics.com. 2012. *Halbach Arrays.* [online] Available at: <https://www.kjmagnetics.com/blog.asp?p=halbach-arrays> [Accessed April 24, 2022].

[4] GENERAL SERVICES. (1984, April). FEDERAL STANDARD SCREW - THREAD STANDARDS FOR FEDERAL SERVICES. Office of Federal Supply and Services.

[5] Byrne, B. W., & Houlsby, G. T. (2015). Helical piles: An Innovative Foundation design option for offshore wind turbines. *Philosophical Transactions of the Royal Society A: Mathematical, Physical and Engineering Sciences*, *373*(2035), 20140081. https://doi.org/10.1098/rsta.2014.0081